Phenylalanine exacerbates psoriasiform inflammation through NF-κB-mediated dendritic cell activation and Th17 polarization

YAOHAN XU[1*], JING PAN[1*], JIE CHEN[2*], YUTAO ZHU[3], MIAOLIAN CAI[1], ZEYU MA[4], SIJI CHEN[1], TIANZE YU[1], YUSHU WEI[1], JINGYING PAN[1], KUNLIANG LUO[5], YINJING SONG[1], STIJN VAN DER VEEN[1,6] and HAO CHENG[1]

[1]Department of Dermatology and Venereology, Sir Run Run Shaw Hospital, Zhejiang University School of Medicine, Hangzhou, Zhejiang 310016, P.R. China; [2]Department of Dermatology, Zhuji People's Hospital, Zhuji Affiliated Hospital of Wenzhou Medical University, Zhuji, Zhejiang 311800, P.R. China; [3]Liangzhu Laboratory, Zhejiang University School of Medicine, Hangzhou, Zhejiang 311121, P.R. China; [4]Department of Gastroenterology, Sir Run Run Shaw Hospital, Zhejiang University School of Medicine, Hangzhou, Zhejiang 310016, P.R. China; [5]Department of Dentistry, Sir Run Run Shaw Hospital, Zhejiang University School of Medicine, Hangzhou, Zhejiang 310016, P.R. China; [6]Department of Microbiology, School of Medicine, Zhejiang University, Hangzhou, Zhejiang 310058, P.R. China

Received February 9, 2026; Accepted June 2, 2026

DOI: 10.3892/ijmm.2026.5921

Abstract. Metabolic dysregulation has been increasingly recognized as a key driver in the pathogenesis of psoriasis; however, the specific mechanistic contributions of amino acid perturbations remain poorly understood. The present study, through comprehensive metabolomic profiling, observed a marked accumulation of phenylalanine in both the circulation and skin lesions of psoriatic mice. Notably, a high-phenylalanine diet exacerbated psoriasiform skin inflammation of imiquimod-induced psoriasis, whereas dietary restriction of phenylalanine or administration of L-type amino acid transporter inhibitors effectively alleviated skin inflammation. Mechanistically, transcriptome sequencing of dendritic cells identified phenylalanine as a potent metabolic trigger. The present analysis revealed that high phenylalanine levels alone significantly elevated the baseline expression of notable pro-inflammatory cytokines and this inflammatory response was further amplified in the presence of imiquimod. The present study determined that this pro-inflammatory effect was mediated through the NF-κB signaling pathway, which subsequently promoted the differentiation of T helper 17 cells. Collectively, the present findings uncovered a previously unrecognized metabolic checkpoint in psoriasis and suggested that restriction of phenylalanine represents a promising, non-toxic adjunctive therapeutic strategy for the clinical management of psoriasis.

Correspondence to: Professor Hao Cheng, Department of Dermatology and Venereology, Sir Run Run Shaw Hospital, Zhejiang University School of Medicine, 3 Qingchun Road, Hangzhou, Zhejiang 310016, P.R. China
E-mail: chenghao1@zju.edu.cn

Professor Stijn van der Veen, Department of Microbiology, School of Medicine, Zhejiang University, 866 Yuhangtang Road, Hangzhou, Zhejiang 310058, P.R. China
E-mail: stijnvanderveen@zju.edu.cn

*Contributed equally

Key words: psoriasis, phenylalanine, amino acid metabolism, inflammatory cytokines, dendritic cells

Introduction

Psoriasis is a chronic autoimmune skin disorder characterized by marked keratinocyte proliferation and inflammatory infiltration (1,2). While IL-23/IL-17-targeted biologics (e.g., guselkumab, secukinumab) have proven beneficial in psoriasis treatment, a notable proportion of patients exhibit partial or no response (3). Furthermore, long-term management of psoriasis is frequently complicated by drug resistance and infection risks (4,5). Thus, a deeper understanding of the molecular mechanisms governing immune activation in the psoriatic microenvironment is imperative.

Beyond the established immunological pathways, such as the IL-23/Th17 axis and TNF-α signaling, increasing evidence has indicated the crucial role of metabolic reprogramming in psoriasis pathogenesis (6-8). Recent studies have highlighted systemic metabolic comorbidities in patients with psoriasis, including obesity, diabetes and cardiovascular risk (9,10), suggesting systemic 'metabolic syndrome' of the skin. While lipid and glucose metabolism have been extensively reviewed in this context, the role of amino acid metabolism remains comparatively underexplored (11-13).

Perturbations of amino acid metabolism are widespread in psoriasis, which are also positively associated with the severity of psoriatic lesions and psoriasis relapse (14). Furthermore, treatment with biological agents targeting TNF-α, IL-12/23 and IL-17A has been shown to normalize these metabolic

disturbances, highlighting the potential importance of amino acids in the pathogenesis of psoriasis (15,16). Notably, the levels of the key amino acid phenylalanine are elevated both in psoriatic skin lesions and the plasma of affected individuals (15,17). Although its dysregulation is implicated in a number of metabolic disorders, including type 2 diabetes (18) and age-associated cardiac dysfunction (19), its role in psoriasis remains largely unexplored.

Within the complex immune landscape of psoriasis, dendritic cells (DCs) occupy a central role, orchestrating the transition from innate to adaptive immunity (20). Recent evidence has highlighted that intracellular lipid accumulation resulting from impaired autophagy, as well as altered amino acid availability that hyperactivates nutrient-sensing pathways including mTOR, markedly disrupts intracellular homeostasis (21,22). This overarching metabolic rewiring forces DCs into an overmatured state and lowers their immune activation threshold. Consequently, when these metabolically primed DCs recognize pathogen- or damage-associated molecular patterns through surface toll-like receptors, they exhibit hyper-responsive behaviors. This hypersensitization leads to an aberrantly amplified activation of the downstream NF-κB signaling cascade, which serves as the core mechanism driving IL-23 secretion (23,24). Consequently, DCs not only initiate and amplify the inflammatory response through the secretion of pro-inflammatory cytokines, including IL-6, IL-23 and IL-1β, but also influence T-cell differentiation, particularly toward the T helper 17 (Th17) phenotype driven by IL-23 (25). Therefore, identifying upstream mechanisms that govern DC activation and curb their cytokine output represents an important frontier for developing therapeutic strategies aimed at achieving long-term remission.

Therefore, the present study was designed to bridge the gap between systemic metabolic perturbations and local immune dysregulation in psoriasis. Using metabolomic profiling, the study sought to investigate phenylalanine accumulation in both the circulation and cutaneous lesions of psoriatic mice, and to elucidate the underlying metabolic perturbation. Furthermore, by manipulating phenylalanine availability *in vivo* and *in vitro*, the study aimed to delineate the mechanistic association between phenylalanine and NF-κB signaling in DCs, and to explore its role in driving the pathogenic IL-23/IL-17 axis, thereby providing a mechanistic rationale for dietary intervention as an adjunctive therapy for psoriasis.

Materials and methods

Animal studies. A total of 47 male C57BL/6 mice (8 weeks old; average weight, 22 g) were procured from the Shanghai SLAC Laboratory Animal Center (Shanghai, China) and housed at the Sir Run Run Shaw Hospital, Zhejiang University School of Medicine (Hangzhou, China). The mice were maintained in a specific pathogen-free facility under controlled environmental conditions (temperature, 22±2˚C; relative humidity, 50±10%; and a 12-h light/dark cycle) with *ad libitum* access to sterile water and their respective diets (standard chow or customized diets as detailed below). The animal study protocols were approved by the Animal Research Ethical Committee of the Sir Run Run Shaw Hospital, Zhejiang University School of Medicine (approval no. SRRSH2025-0047). To address distinct experimental objectives, the mice were randomly assigned to specific cohorts as follows: i) For metabolomics profiling, mice were fed with standard chow and randomly divided into a normal control (NC) group and an imiquimod (IMQ)-induced model group (n=6 per group); ii) to evaluate the efficacy of phenylalanine (Phe) diets, mice were randomly assigned to three groups (n=5 per group) and fed diets containing either 0.25%, 1% (serving as the baseline control) or 2% Phe, which were manufactured by Hangzhou Hangsi Biotechnology Co., Ltd. (Table SI); and iii) For the *in vivo* L-type amino acid transporter 1 (LAT1) inhibition experiment, mice were allocated into four groups (n=5 per group). For the relevant experimental groups, the LAT1 inhibitor JPH203 (cat. no. s8667; Selleck Chemicals) was administered through subcutaneous injection at a dose of 50 mg/kg.

To establish mouse models of psoriasis, IMQ cream (Sichuan Med-Shine Pharmaceutical Co., Ltd.) was applied topically for 5 consecutive days. For the back skin model, 62.5 mg IMQ cream was applied daily to the shaved dorsal skin. For the ear inflammation model, to ensure consistent and complete absorption of the full dose and minimize the risk of medication loss due to animal grooming, 25 mg IMQ cream was applied evenly across both the dorsal and ventral surfaces of the right ear. All mice were weighed and recorded before the induction of psoriasis. Health status and behavioral patterns of all animals were monitored twice daily (morning and evening) during the 6-day study period to assess disease progression and treatment efficacy. An objective scoring system was used to score the severity of skin inflammation based on the clinical Psoriasis Area and Severity Index (PASI) (26). Next, erythema, thickening, and scaling were rated on a 0-4 scale, where 0, 1, 2, 3 and 4 indicated no symptoms, mild, moderate, severe or extremely severe symptoms, respectively. The cumulative scores served as the severity of inflammation index (scale 0-12). The researchers were blinded during the experiment and data analysis.

To monitor the dynamic progression of psoriasiform inflammation, the macroscopic clinical severity of the mouse skin was evaluated and recorded daily. The final PASI scores analyzed and presented in the present figures were recorded on day 6 of the experiment, prior to euthanasia. On day 6, all terminal procedures were performed in a strict sequence. Mice were euthanized through CO_2 asphyxiation with a controlled displacement rate of 30% of the chamber volume per min and mortality was strictly verified by determining the absence of heartbeat and respiration. Immediately following the confirmation of mortality, blood was collected through retro-orbital bleeding and lesional skin tissues and plasma were subsequently harvested for further histological and metabolic analyses. The excised spleens were immediately weighed and the spleen index was calculated as the ratio of spleen weight to body weight. The acanthosis thickness was analyzed using ImageJ software (version 1.53; National Institutes of Health) and the thickness of the ear skin was measured with a vernier caliper.

Metabolomics profile analysis. Mouse tissues and plasma were collected and analyzed by Wuhan Metware Biotechnology Co., Ltd. Specifically, 100 mg tissue or 100 μl plasma was homogenized in 500 μl 70% aqueous methanol solution. The

mixture underwent a 3 min vortex-mixing step at 2,500 rpm, followed by centrifugation (13,800 x g, 10 min, 4˚C). A total of 300 μl supernatant was isolated into fresh vials for liquid chromatography (LC)-mass spectrometry (MS) analysis. To ensure analytical stability, quality control samples were generated by combining equal aliquots from every individual specimen and handled identically.

Sample extracts were analyzed using an LC-electrospray ionization (ESI)-MS/MS system (ExionLC™ AD UPLC coupled with a QTRAP® 6500+ System; SCIEX). The instrument operated under both positive (5,500 V) and negative (-4,500 V) ion spray modes utilizing an ESI Turbo Ion-Spray (SCIEX) interface (source temperature: 550˚C and curtain gas: 35.0 psi), managed using Analyst® (version 1.6; SCIEX) software. Multiple reaction monitoring transitions were continuously optimized for each elution window of target amino acids.

Data analysis. Raw mass spectrometry outputs were transformed into MzXML files utilizing ProteoWizard MSConvert (version 3.0; http://proteowizard.sourceforge.net) prior to XCMS integration (using the 'xcms' package on the R platform; version 4.1.2; https://bioconductor.org/packages/xcms). Strict thresholds [variable importance in projection (VIP) >1 and P<0.05] were applied within the Partial Least Squares Discriminant Analysis model to filter differential metabolites. Pathway impact assessments were conducted using MetaboAnalyst (version 5.0; https://www.metaboanalyst.ca), where pathways exhibiting an impact factor >0.1 were deemed highly significant.

Immunohistochemical and histological analysis. Mouse skin samples were immersed in 4% paraformaldehyde for optimal fixation at room temperature for 24 h. Tissues were subsequently dehydrated, cast into paraffin blocks and microtomed into 5-μm cross-sections. H&E staining was carried out following the manufacturer's instructions (Beyotime Biotechnology). For immunofluorescence assays, the sections were first deparaffinized in xylene and rehydrated using a descending ethanol gradients. Heat-mediated antigen unmasking was performed at 95˚C for 15 min in a pH 6.0 citrate buffer. To prevent non-specific binding, slides were treated with a 5% BSA solution (Beyotime Biotechnology) enriched with 0.1% Triton X-100 for 1 h at room temperature. Primary antibody incubation with anti-p-p65 (1:200 dilution; cat. no. 3033S; Cell Signaling Technology, Inc.) occurred overnight at 4˚C. After rigorous washing with PBS. specimens were exposed to CoraLite® Plus 488-conjugated AffiniPure goat anti-rabbit IgG (H+L) (1:200 dilution; cat. no. RGAR002; Proteintech Group, Inc.) for detection of p-p65, for 1 h at room temperature in the dark. Subsequently, specimens were incubated with anti-CD11c (Alexa Fluor® 555 conjugate) (1:200 dilution; cat. no. 64675S; Cell Signaling Technology, Inc.) overnight at 4˚C. CD11c was visualized directly via its Alexa Fluor® 555 conjugate without requiring a secondary antibody. All images were eventually captured utilizing a digital slide scanning system (Konfoong Bioinformation Tech Co., Ltd.).

Skin cell isolation and flow cytometric analysis. Single cells from the ear were generated according to the methods of a previous study (27). To prevent non-specific Fc receptor binding, single-cell suspensions were pre-treated with the anti-mouse CD16/32 antibody (1:500 dilution; cat. no. 553141; BD Biosciences) on ice for 20 min prior to the surface marker labeling. The antibodies (all used at 1:500 dilution) for flow cytometry included allophycocyanin (APC)-A700-CD45 (56-0454081; eBioscience; Thermo Fisher Scientific, Inc.), FITC-CD3 (cat. no. 11-0032-82; eBioscience; Thermo Fisher Scientific, Inc.), BV650-CD11b (cat. no. 416-0112-80; eBioscience; Thermo Fisher Scientific, Inc.) and BV421-LY6G (cat. no. 404-9668-80; eBioscience; Thermo Fisher Scientific, Inc.). The Zombie Aqua™ Fixable Viability Kit (cat. no. 423101; BioLegend, Inc.) was also used. After washing, the cells were assayed with a CytoFLEX LX flow cytometer (Beckman Coulter, Inc.) and the data were analyzed using FlowJo software (version 10; BD Biosciences).

RNA extraction and reverse transcription-quantitative PCR (RT-qPCR). Total RNA was isolated from harvested skins or DCs using RNAiso Plus (Takara Bio, Inc.). Reverse transcription for cDNA synthesis was conducted utilizing the PrimeScript™ RT Reagent Kit (cat. no. RR037A; Takara Bio, Inc.) following the provided technical guidelines. RT-qPCR was conducted using the Hieff™ qPCR SYBR Green Master Mix (cat. no. 11201ES08; Shanghai Yeasen Biotechnology Co., Ltd.) on a LightCycler® 480 system (Roche Diagnostics GmbH). The thermocycling program commenced with a 5 min pre-denaturation at 95˚C, sequentially followed by 40 cycles (95˚C for 10 sec and 60˚C for 30 sec). Target gene expression levels were normalized against the housekeeping gene β-actin leveraging the $2^{-\Delta\Delta Cq}$ method (28). Primer sequences are listed in Table SII.

Preparation of bone marrow-derived DCs (BMDCs) and treatments. To isolate primary cells for both BMDC and naïve $CD4^+$ T cell experiments, healthy and untreated male C57BL/6 donor mice (aged 6-8 weeks) obtained from the Shanghai SLAC Laboratory Animal Center, (Shanghai, China) were utilized. A total of 10 donor mice were euthanized using CO_2 asphyxiation (at a displacement rate of 30% of the chamber volume per min) and mortality was verified by cervical dislocation. To obtain sufficient cell yields, biological replicates for the following *in vitro* assays were generated using pooled samples from these donor mice.

To prepare BMDCs, femurs and tibias were flushed with RPMI-1640 medium (Gibco; Thermo Fisher Scientific, Inc.) to collect bone marrow. The cell pellet was subsequently resuspended in red cell lysis buffer (Beyotime Biotechnology) for 3 min. The primary culture system consisted of RPMI-1640 fortified with 10% FBS (CellMax Technologies AB), 1% penicillin-streptomycin, 50 μM β-mercaptoethanol (cat. no. abs9592; Absin Bioscience, Inc.), 20 ng/ml GM-CSF (cat. no. 315-03; PeproTech®; Thermo Fisher Scientific, Inc.) and 10 ng/ml recombinant mouse IL-4 (cat. no. 214-14; PeproTech®; Thermo Fisher Scientific, Inc.). On days 3 and 5, half of the old culture medium was carefully removed and replaced with an equal volume of fresh medium. All cells were cultured at 37˚C in a 5% CO_2 incubator. On day 6, BMDCs were used for relevant experiments. All *in vitro* pharmacological treatments were conducted at 37˚C in a 5% CO_2 incubator. For

in vitro stimulation, IMQ powder (cat. no. R837; InvivoGen) was dissolved in sterile water and added to the culture medium at a final concentration of 10 μg/ml. For inhibitor treatments, cells were incubated with the NF-κB inhibitor BAY11-7082 (10 μM; MedChemExpress) or the LAT1 inhibitor JPH203 (100 μM; Selleck Chemicals) for 2 h.

To detect maturation of BMDCs, expression of CD80, CD86 and major histocompatibility Complex (MHC)-II was analyzed on CD11c-positive cells using APC-labelled anti-CD80 (cat. no. 104713; BioLegend, Inc.), primary binding-labelled anti-CD86 (cat. no. 105021; BioLegend, Inc.), phycoerythrin (PE)-labelled anti-MHCII (cat. no. 12-5321-81, eBioscience; Thermo Fisher Scientific, Inc.) and PE-Cy7-labelled anti-CD11c (cat. no. 117317, BioLegend, Inc.) antibodies (all used at a 1:500 dilution). The incubation was performed on ice for 20 min in the dark. After antibody staining, cells were washed and analyzed with a CytoFLEX LX flow cytometer (Beckman Coulter, Inc.).

BMDC supernatant and T cell co-culture. On day 6, BMDCs were pre-treated with phenylalanine (1 mM) for 48 h at 37˚C in a humidified incubator containing 5% CO_2, followed by incubation with IMQ 10 μg/ml for 24 h to harvest the supernatant. Naïve $CD4^+$ T cells were isolated from the spleens of C57BL/6 mice using an isolation kit (cat. no. 19765A, Stemcell Technologies, Inc.). A total of 200 μl BMDC supernatant was used to resuspend naïve $CD4^+$ T cells for co-culture for 72 h. Differentiated T cells were stimulated with 750 ng/ml ionomycin (cat. no. 5608212; PeproTech®; Thermo Fisher Scientific, Inc.), 50 ng/ml phorbol 12-myristate 13-acetate (cat. no. S1819; Beyotime Biotechnology) and brefeldin A (cat. no. 00-4506-51; eBioscience; Thermo Fisher Scientific, Inc.) for another 4 h at 37˚C. The cells were then collected, stained with PE-labelled anti-CD4 (cat. 17-0041-82; eBioscience; Thermo Fisher Scientific, Inc.) and APC-labelled anti-IL-17A (cat. 17-7177-81; eBioscience, Thermo Fisher Scientific, Inc.) antibodies (both at a 1:500 dilution) on ice for 20 min in the dark. The stained cells were then analyzed on a CytoFLEX LX flow cytometer (Beckman Coulter, Inc.).

RNA sequencing (RNA-seq) data processing. Total RNA was isolated from harvested tissues or DCs leveraging the RNAiso Plus reagent (Takara Bio, Inc.) as directed by the manufacturer. RNA purity and integrity were verified using a NanoDrop 2000 spectrophotometer and an Agilent 2100 Bioanalyzer (RIN >7.0). Transcriptomic libraries were constructed, verified using an Agilent 2100 Bioanalyzer, and subsequently subjected to 2x150 bp paired-end sequencing. The sequencing runs were executed on the Illumina NovaSeq™ X Plus system (Illumina, Inc.) at a final loading concentration of 1.5 nM by LC-Bio Technologies (Hangzhou) Co., Ltd. The 'DESeq2' package (29) was utilized within the R platform (version 4.1.2) for transcriptomic comparisons between specific groups, whereas the 'edgeR' algorithm (30) was employed for evaluating individual sample variations. Differentially expressed genes (DEGs) were defined by a false discovery rate (FDR) <0.05 and an absolute fold change ≥2. DEGs were then subjected to enrichment analysis of Gene Ontology (GO) functions and Kyoto Encyclopedia of Genes and Genomes (KEGG) pathways.

Western blotting. BMDCs were lysed in standard RIPA buffer (Beyotime Biotechnology) to liberate total cellular proteins. Lysates were subjected to low-temperature centrifugation (10,000 x g, 4˚C, 20 min) to clear cellular debris. Protein quantification was executed using a BCA reagent kit (cat. no. FD2001; Fdbio Science). Equivalent protein masses (30 μg per lane) were resolved using 12% SDS-PAGE and electrically blotted onto 0.22 μm PVDF transfer membranes. The membranes were blocked with 5% non-fat dairy milk for 1 h at room temperature prior to overnight incubation at 4˚C with distinct primary antibodies: anti-NF-κB p65 (1:1,000 dilution; cat. no. 8242; Cell Signaling Technology, Inc.), phosphorylated (p)-NF-κB p65 (Ser536; 1:1,000 dilution; cat. no. 3033; Cell Signaling Technology, Inc.), anti-IκBα (1:1,000 dilution; cat. no. 4814; Cell Signaling Technology, Inc.) and anti-p-IκBα (Ser32; 1:1,000 dilution; cat. no. 2859; Cell Signaling Technology, Inc.). An anti-β-tubulin antibody (1:1,000 dilution; cat. no. AF2839; Beyotime Biotechnology) was used as the loading control. The subsequent day, blots were probed with an HRP-conjugated goat anti-rabbit secondary antibody (1:5,000 dilution; cat. no. A0208; Beyotime Biotechnology) for 1 h at room temperature. For the detection of phosphorylated and total proteins (such as p-p65/p65 and p-IκBα/IκBα) on the same membrane, the PVDF membranes were first probed for the phosphorylated proteins, then stripped using a commercial stripping buffer (cat. no. FD0050; Fdbio Science), blocked again and reprobed for the respective total proteins. Immunoreactive bands were optically captured using a VILBER Fusion FX7 imaging system (Vilber Lourmat) supported by a specialized chemiluminescent substrate (cat. no. FD8030; Fdbio Science).

Statistical analysis. All quantitative datasets were processed and visualized utilizing GraphPad Prism (version 9.0; Dotmatics). For statistical comparisons involving two independent cohorts, a two-tailed Student's t-test was executed. When evaluating datasets containing >2 experimental groups, either one-way or two-way ANOVAs were applied, followed by Tukey's post-hoc test for multiple pairwise comparisons. $P<0.05$ was considered to indicate a statistically significant difference. Data are presented as the mean ± SEM.

Results

Psoriasis progression is associated with abnormal phenylalanine metabolism. To investigate the metabolic landscape associated with psoriasis progression, untargeted metabolomics profiling was performed on skin samples from IMQ-induced psoriasis-like mouse models and NCs (Fig. 1A). PCA revealed distinct metabolic clustering, indicating a shift in the metabolic profile following IMQ treatment (Fig. 1B). Specifically, out of 14,887 detected features, 3,506 significantly upregulated and 1,160 significantly downregulated metabolites were identified in the psoriatic skin (Fig. 1C). To interpret the biological importance of these shifts, KEGG pathway enrichment analysis was performed. The results demonstrated that the altered metabolites were predominantly enriched in amino acid metabolism pathways, including 'arginine biosynthesis', 'histidine metabolism' and notably, 'phenylalanine metabolism' (Fig. 1D). Given the high enrichment ratio and statistical

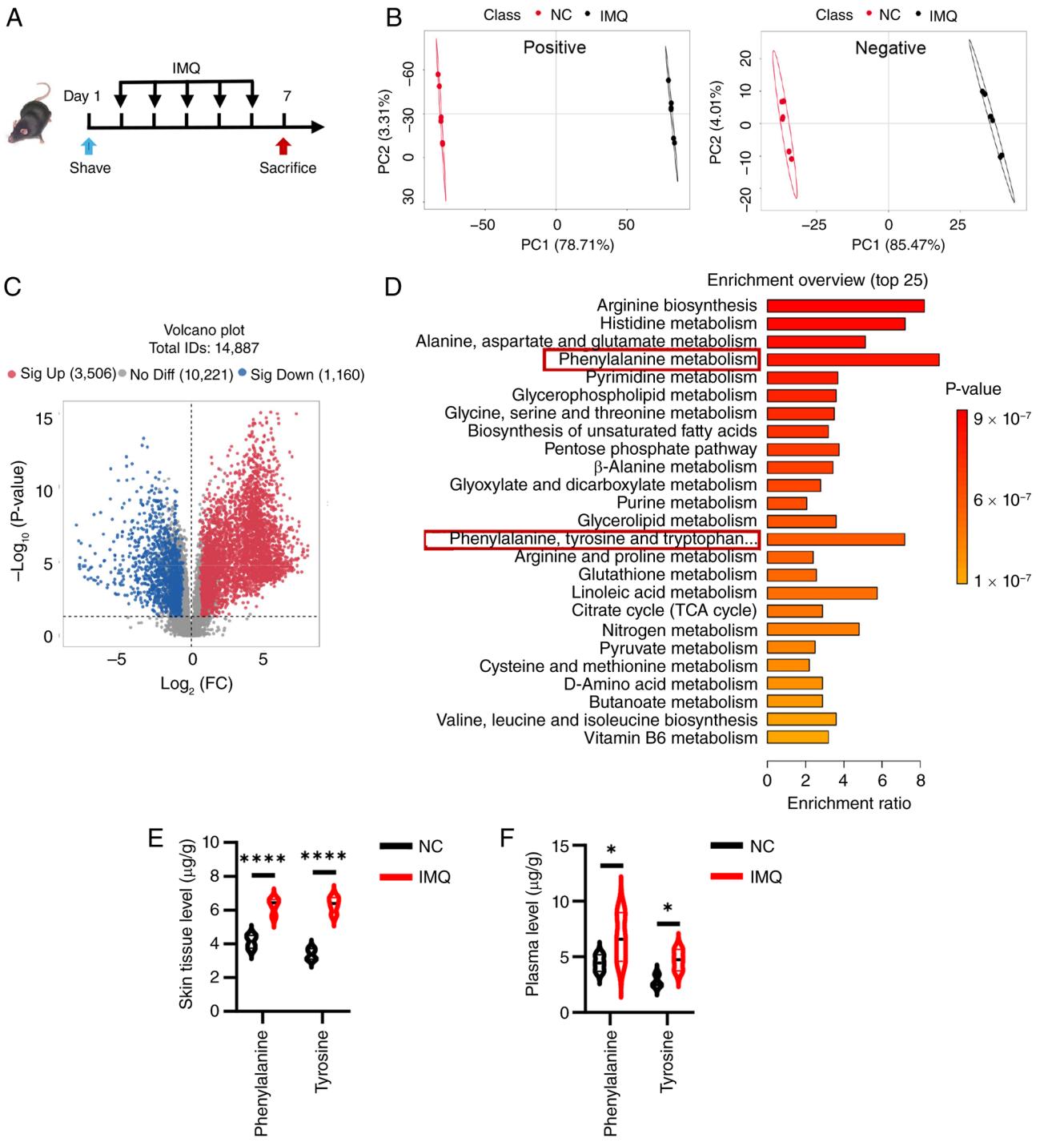

Figure 1. Psoriasis progression is associated with aberrant phenylalanine metabolism in IMQ-induced mice. (A) Schematic of the experimental design for the IMQ-induced psoriasis model (n =5 mice/group). (B) PC analysis score plots exhibiting distinct metabolic clustering and separation between the NC group and the IMQ model group in both positive and negative ion modes. (C) Volcano plots showing the differential abundance of total identified metabolites (n=14,887). Red dots represent significantly upregulated metabolites (n=3,506), blue dots represent significantly downregulated metabolites (n=1,160), variable importance in projection >1, P<0.05 and absolute FC >1.2. (D) Overview of the top 25 terms in the metabolic enrichment analysis of the differential metabolites. Absolute quantification of phenylalanine and tyrosine levels in (E) skin tissue (μg/g) and (F) plasma (μg/ml) using targeted metabolomics. Data are presented as the mean ± SEM. Statistical significance between the two groups was determined using an unpaired two-tailed Student's t-test. *P<0.05 and ****P<0.0001. IMQ, imiquimod; NC, normal control; FC, fold change; ns, not significant; PC, principal component.

significance associated with phenylalanine metabolism, this pathway was selected for further validation.

These untargeted findings were next corroborated using targeted quantitative metabolomics to measure absolute concentrations of phenylalanine and its downstream metabolite, tyrosine. Consistent with the present initial metabolomics screening, phenylalanine and tyrosine levels were found to be significantly elevated in the skin lesions of IMQ-treated mice compared with NC group (Fig. 1E). Furthermore, plasma analysis also revealed a significant systemic increase in circulating phenylalanine and tyrosine levels (Fig. 1F). These findings collectively suggested that the progression of psoriasis was

closely associated with aberrant phenylalanine metabolism (Fig. S1), leading to the accumulation of both phenylalanine and tyrosine systemically and locally in skin lesions.

Phenylalanine exacerbates IMQ-induced mouse psoriasis-like skin lesions. Having identified phenylalanine accumulation as a metabolic hallmark of psoriasis, the concentration of phenylalanine was adjusted in the diet of mice during psoriasis modeling to determine whether altering systemic phenylalanine levels functionally modulates disease outcome (19). C57BL/6 mice were acclimated to diets containing varying concentrations of phenylalanine (0.25, 1 or 2%) for 1 week prior to and during the course of IMQ treatment (Fig. 2A). Notably, these dietary modifications did not significantly affect general health or body weight before IMQ treatment (Fig. 2B). However, after IMQ application, phenotypic assessment revealed a significant dose-dependent effect of phenylalanine on skin inflammation. Mice fed a high-phenylalanine diet (2%) exhibited exacerbated psoriasis-like lesions characterized by severe erythema, heavy scaling and skin thickening. Conversely, dietary restriction of phenylalanine (0.25%) significantly alleviated these clinical manifestations compared with the standard diet (1%) group (Fig. 2C). This observation was quantified by PASI scores, which exhibited a clear dose-dependent trajectory (Figs. 2D and S2). Histological analysis of the dorsal skin further demonstrated these findings: High dietary phenylalanine induced pronounced epidermal hyperplasia (acanthosis) and inflammatory cell infiltration, whereas phenylalanine restriction effectively attenuated these pathological changes (Fig. 2E and F). To characterize the inflammatory milieu driven by phenylalanine, the gene expression of key psoriasis-associated cytokines in the skin were analyzed. It was found that elevated dietary phenylalanine significantly promoted the gene expression levels of *Il1b*, *Il6* and C-X-C motif chemokine ligand (*Cxcl*-)1, as well as the key psoriasis drivers *Il12b*, *Il23a* and *Il17a* (Fig. 2G). Consistent results were observed in the ear skin, whereby high phenylalanine aggravated ear swelling and histological severity, accompanied by a significant increase in ear thickness (Fig. 2H-J). To further establish the pathological severity and terminal phenotype of the disease model, the infiltration of neutrophils was evaluated, which serve as a well-established marker of psoriasis severity (31). Flow cytometry analysis of single-cell suspensions from the ear skin revealed that dietary phenylalanine significantly dose-dependently increased the infiltration of neutrophils (Fig. 2K and L). In summary, these results indicated that phenylalanine acted as an aggravating factor in psoriasis, likely by amplifying pro-inflammatory cytokine production and promoting immune cell recruitment to skin lesions.

LAT1 inhibitor JPH203 mitigates phenylalanine-driven psoriatic inflammation. To validate the therapeutic potential of restricting cellular phenylalanine availability, LAT1, the primary transporter for large neutral amino acids, was targeted. JPH203, a selective high-affinity LAT1 inhibitor, was utilized in mice subjected to the high-phenylalanine diet and IMQ challenge (Fig. 3A). Notably, administration of JPH203 alone to healthy mice did not induce any cutaneous abnormalities or toxicity. Aligning with the present hypothesis, JPH203 exerted a potent protective effect. Treatment with this inhibitor markedly abrogated the exacerbating impact of dietary phenylalanine. Clinically, this was evidenced by a marked reduction in erythema and scaling compared with the vehicle-treated IMQ group (Fig. 3B). Consistent with these macroscopic observations, histological assessment of the dorsal skin revealed that JPH203 effectively significantly pathological epidermal thickening (Fig. 3C). Quantitative analyses further demonstrated these protective effects, demonstrating significant reductions in PASI scores (Figs. 3D and S3) and epidermal acanthosis thickness (Fig. 3E). Similarly, in the ear skin model, JPH203 treatment alleviated tissue swelling and restored epidermal architecture, characterized by reduced hyperkeratosis and fewer pustules (Fig. 3F), as well as a significant reduction in ear thickness (Fig. 3G). At the cellular level, flow cytometry analysis revealed that JPH203 treatment effectively suppressed the immune response, leading to a significant reduction in the frequency of infiltrating neutrophils in skin lesions (Fig. 3H and I). Furthermore, systemic inflammation was assessed by examining the spleen. While IMQ treatment induced significant splenomegaly, JPH203 co-administration normalized both spleen size and the spleen index (Fig. 3J and K). Collectively, these findings demonstrated that blocking phenylalanine transport through JPH203 effectively disrupted the phenylalanine-dependent inflammatory loop, providing therapeutic benefits both locally and systemically.

Phenylalanine promotes expression of psoriasis-associated cytokines and chemokines in DCs. DCs serve as key orchestrators in the initiation of psoriasis, primarily by driving the IL-23/IL-17 axis (32). The present *in vivo* findings demonstrated that systemic phenylalanine markedly aggravated IMQ-induced psoriasis-like dermatitis. To elucidate the molecular basis of this effect, RNA-seq was performed on BMDCs exposed to phenylalanine in the presence or absence of IMQ stimulation. Transcriptomics analysis revealed that phenylalanine exposure alone was sufficient to notably alter the DC landscape (Fig. 4A). Compared with vehicle controls, phenylalanine treatment significantly upregulated 116 genes (Fig. 4B). KEGG enrichment analysis showed phenylalanine significantly regulated genes associated with the 'cytokine-cytokine receptor interaction', 'NOD-like receptor signaling pathway' and 'NF-κB signaling pathway' (Fig. 4C). Notably, in the context of inflammatory challenge (IMQ stimulation), phenylalanine acted as a potent amplifier. Co-treatment with phenylalanine and IMQ induced a distinct transcriptional profile compared with IMQ alone. Differential expression analysis highlighted further upregulation of 245 genes, including key pro-inflammatory mediators such as *Il1a*, *Il1b*, *Il6* and *Cxcl1-3*. Functional enrichment analysis determined that phenylalanine potentiated pathways key in psoriasis pathogenesis, including the 'IL-17 signaling pathway' and 'cytokine-cytokine receptor interaction' (Fig. 4D).

To validate these transcriptomic signatures, qPCR was performed on independent samples. Consistent with the RNA-seq data, phenylalanine treatment alone significantly increased the basal expression of *Il6* and *Il12b*, while only slightly elevating *Il1b* and *Il23a* levels without statistical significance. Notably, it significantly and synergistically

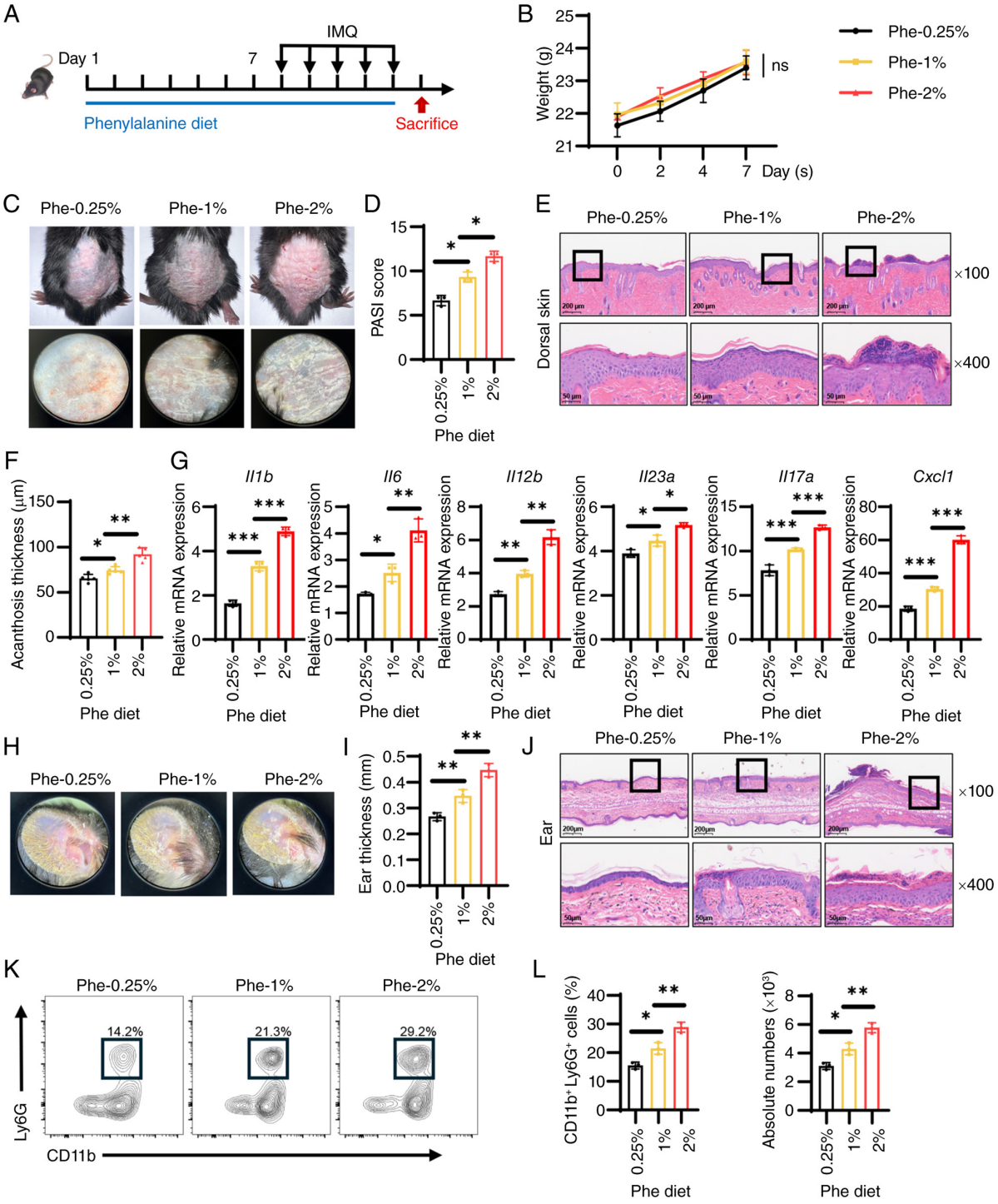

Figure 2. Dietary phenylalanine exacerbates IMQ-induced psoriasis-like dermatitis in a dose-dependent manner. (A) Schematic representation of the dietary intervention: Mice were fed diets containing 0.25% (low), 1% (normal) or 2% (high) Phe for 7 days prior to and during IMQ application (n=5/group). (B) Recorded body weights of mice fed with Phe diet prior to IMQ application. (C) Representative phenotypic images of dorsal skin lesions across dietary groups after IMQ treatment. (D) PASI scores of the mice in each group evaluated on day 6. (E) Representative H&E-stained sections of the dorsal skin (scale bars, 50 and 200 μm; the black rectangles indicate the regions of interest magnified in the 400x views below). (F) Histological quantification of epidermal thickness (acanthosis) in dorsal skin lesions. (G) Reverse transcription-quantitative PCR analysis of pro-inflammatory cytokines (*Il1b*, *Il6*, *Il12b*, *Il23a*, and *Il17a*) and chemokine *Cxcl1* gene expression in skin tissues. (H) Representative images of ears skin (ventral side). (I) Ear thickness measurement. (J) Representative H&E-stained sections of the ear skin (scale bars, 50 and 200 μm). Flow cytometry analysis showing (K) representative relative percentage and (L) absolute quantification of infiltrating neutrophils ($CD11b^+$ $Ly6G^+$) in ear tissues. Data are presented as the mean ± SEM. Statistical significance was determined using two-way ANOVA (for B and D) or one-way ANOVA (for all others), followed by Tukey's multiple comparisons test. *P<0.05, **P<0.01 and ***P<0.001. IMQ, imiquimod; ns, not significant; Cxcl1, C-X-C motif chemokine ligand 1; Phe, phenylalanine.

enhanced the IMQ-induced expression of these cytokines, as well as the neutrophil-attracting chemokines *Cxcl1*, *Cxcl2* and *Cxcl3* (Fig. 4E). To determine whether this effect was specific to phenylalanine or shared by its downstream metabolites, the impact of tyrosine supplementation was evaluated. While tyrosine also exacerbated the IMQ-induced expression of *Il1b*,

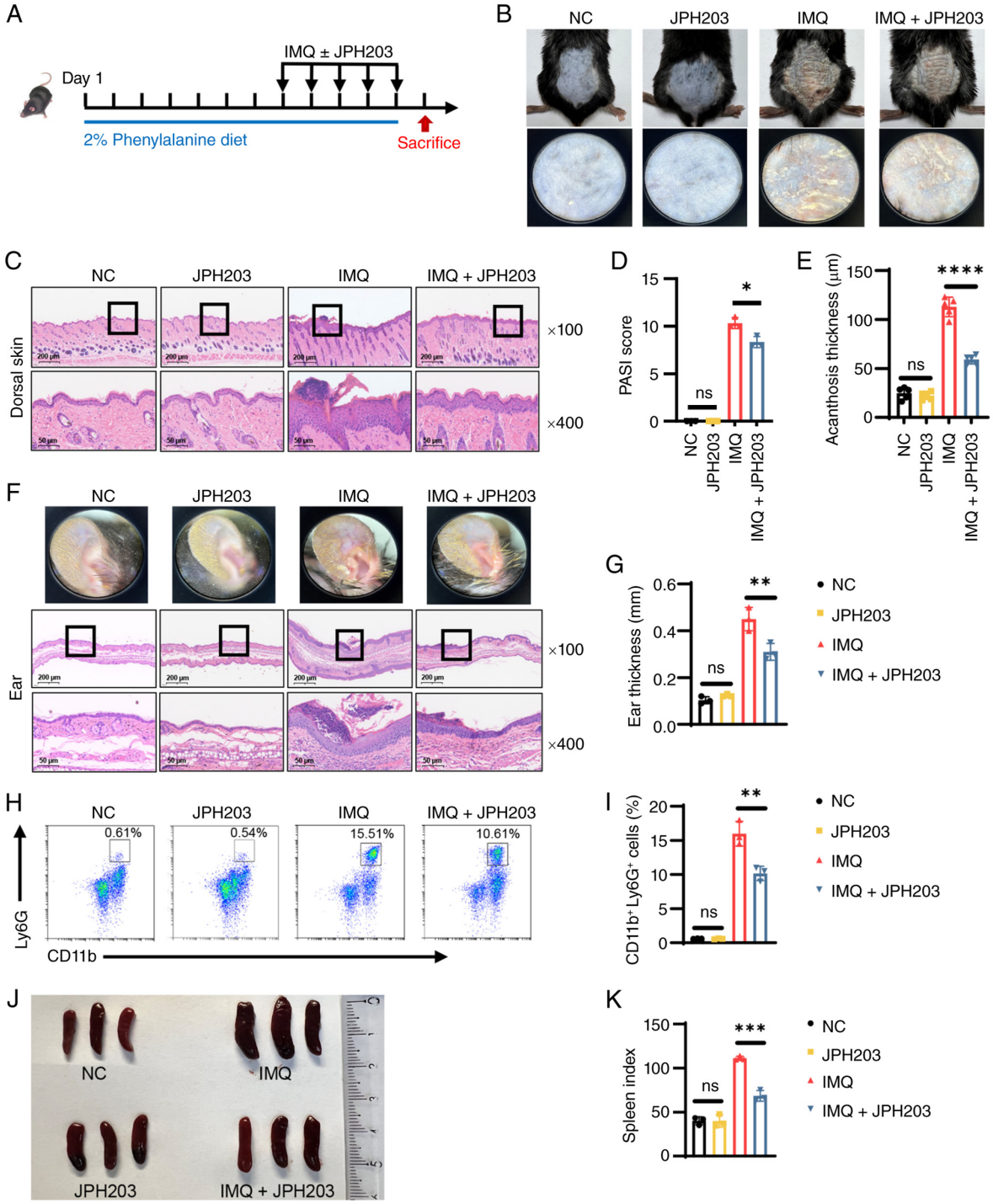

Figure 3. Pharmacological inhibition of L-type amino acid transporter 1 through JPH203 ameliorates psoriatic inflammation in mice. (A) Schematic representation of the psoriasis-like mouse model fed with a high phenylalanine (2%) diet, with or without daily subcutaneous injection of JPH203 (50 mg/kg) or vehicle concurrent with IMQ application. (B) Representative clinical photographs and (C) H&E-stained sections of dorsal skin (scale bars, 50 and 200 μm; the black rectangles indicate the regions of interest magnified in the 400x views below). (D) PASI scores evaluated on day 6. (E) Quantification of epidermal acanthosis thickness in dorsal skin. (F) Representative clinical images of the ear skin (ventral side) and corresponding H&E staining of ear cross-sections (scale bars, 50 and 200 μm; the black rectangles indicate the regions of interest magnified in the 400x views below). (G) Quantification of ear thickness. (H) Flow cytometry analysis of the (I) percentage and total number of infiltrating neutrophils ($CD11b^+$ $Ly6G^+$) in the ears of mice. (J) Representative gross morphology of spleens and (K) quantification of the spleen index. Data are presented as the mean ± SEM. Statistical significance was determined by two-way ANOVA (for D) and one-way ANOVA (for all others) followed by Tukey's multiple comparisons test. *P<0.05, **P<0.01, ***P<0.001 and ****P<0.0001. IMQ, imiquimod; ns, not significant; PASI, Psoriasis Area and Severity Index; NC, normal control.

Il6 and *Il12b*, its effect was notably less potent compared with that of phenylalanine in combination with IMQ (Fig. 4F). This suggested that while tyrosine contributes to the phenotype, phenylalanine itself acted as the primary driver of the hyper-inflammatory state in DCs. Collectively, these data suggest that phenylalanine reprogramed the DC transcriptome, lowering the threshold for activation and amplifying the magnitude of the inflammatory response.

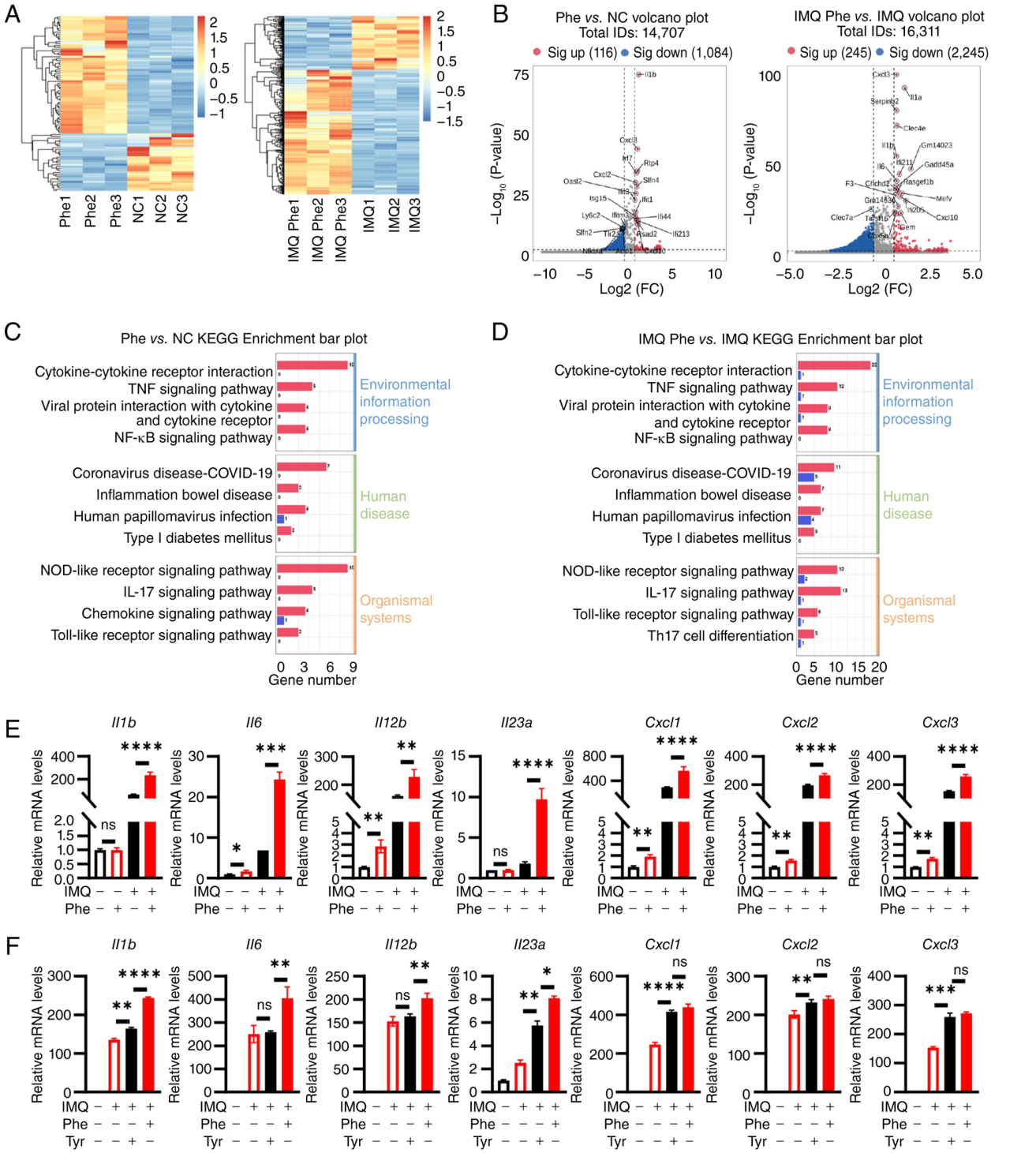

Figure 4. Phe potentiates the inflammatory response in BMDCs. BMDCs were treated with Phe or the vehicle for 48 h, with or without IMQ stimulation, followed by RNA sequencing and qPCR analysis. (A) Hierarchical clustering heatmap of DEGs comparing Phe alone vs. NC and IMQ + Phe vs. IMQ alone. (B) Volcano plots depicting DEGs in Phe vs. NC and IMQ + Phe vs. IMQ comparisons. KEGG pathway enrichment analysis showing top enriched pathways for the upregulated genes in (C) Phe vs. NC and (D) IMQ + Phe vs. IMQ comparisons. (E) RT-qPCR validation of key psoriasis-associated cytokines (*Il1b*, *Il6*, *Il12b* and *Il23a*) and chemokines (*Cxcl1*, *Cxcl2* and *Cxcl3*) across four experimental groups (NC, Phe, IMQ and IMQ + Phe). (F) RT-qPCR analysis comparing the effects of Phe and tyrosine supplementation on cytokine expression under IMQ stimulation. Data are representative of three independent experiments and presented as the mean ± SEM. Statistical significance was determined by two-way ANOVA (for E) and one-way ANOVA (for F), followed by Tukey's multiple comparisons test. *P<0.05, **P<0.01, ***P<0.001 and ****P<0.0001. IMQ, imiquimod; ns, not significant; NC, normal control; DEGs, differentially expressed genes; Cxcl, C-X-C motif chemokine ligand; Phe, phenylalanine; qPCR, quantitative PCR; RT-qPCR, reverse transcription-qPCR; KEGG, Kyoto Encyclopedia of Genes and Genomes; BMDCs, bone marrow-derived dendritic cells; FC, fold change.

Phenylalanine enhances NF-κB activation in dendritic cells to promote cytokine production. To mechanistically validate the present transcriptomic signatures, the NF-κB signaling axis, a central regulator of inflammatory cytokine production (33), was investigated. The activation status of DCs was first examined *in vivo*. Immunofluorescence staining of skin lesions from

mice fed different diets revealed that while the total density of infiltrating DCs ($CD11c^+$) remained comparable across dietary groups (Fig. 5A and B), the activation state was markedly altered. Specifically, the fluorescence intensity of p-$p65^+$ within DCs exhibited an upward trend, though a statistically significant increase was only observed between the 1 and 2% phenylalanine groups (Fig. 5A and C). The signaling kinetics were next dissected *in vitro* using BMDCs. Western blotting analysis demonstrated that phenylalanine treatment independently elevated the basal phosphorylation levels of IκBα and p65. Following the addition of IMQ, the expression of phosphorylated IκBα and p65 were further upregulated (Fig. 5D). Quantification showed that the phosphorylation levels of IκBα and p65 were significantly amplified at numerous time points compared with the controls (Fig. 5E and F). To prove causality, cells were treated with BAY11-7082, a specific NF-κB inhibitor. While phenylalanine strongly potentiated the IMQ-induced expression of *Il1b*, *Il6*, *Il12b*, *Il23a* and *Cxcl1*, pharmacological blockade of NF-κB abrogated this amplification effect (Fig. 5G), determining that the pro-inflammatory action of phenylalanine was dependent on the NF-κB axis. Finally, to determine an association between intracellular signaling to amino acid transport, the LAT1 inhibitor JPH203 was utilized. Western blotting revealed that blocking phenylalanine uptake effectively suppressed hyperactivation of the pathway, evidenced by reduced phosphorylation of IκBα and p65 in JPH203-treated cells (Fig. 5H-J). Consistent with this, JPH203 treatment significantly attenuated gene expression of downstream cytokines and chemokines in phenylalanine-exposed DCs (Fig. 5K). In summary, these data indicated that LAT1-mediated phenylalanine uptake fueled the hyperactivation of NF-κB signaling, thereby drove the excessive production of psoriasis-associated cytokines in DCs.

Phenylalanine exacerbates psoriasis by promoting Th17 cell differentiation and IL-17 cytokine production. DCs serve an important role in immature T cell differentiation and the present data showed that phenylalanine amplified the production of Th17-polarizing cytokines (IL-6, IL-23 and IL-1β) by DCs. The present study hypothesized that this metabolic cue would ultimately exacerbate psoriasis by fueling a Th17-dominant response. To test this *in vivo*, the systemic immune profile of mice fed diets with varying phenylalanine concentrations were analyzed. Flow cytometry analysis of drained lymph nodes revealed a notable dose-dependent expansion of Th17 cells. Mice on the 2% phenylalanine diet exhibited the highest frequency and absolute numbers of Th17 cells among all diet groups (Fig. 6A-C). To determine that this Th17 expansion was mechanistically driven by DC-derived signals rather than a direct effect on T cells, an *in vitro* differentiation assay was performed using DC-conditioned medium. Naïve $CD4^+$ T cells were cultured in supernatants collected from BMDCs that had been subjected to different treatments. Results indicated that the conditioned medium from phenylalanine-primed, IMQ-stimulated DCs possessed a potent capacity to drive Th17 polarization. T cells cultured in this medium exhibited significantly upregulated gene expression of the master transcription factor RAR-related orphan receptor C (*Rorc*) and the effector cytokines *Il17a*, *Il17f* and *Il22* compared with controls (Fig. 6D). This was further corroborated by flow cytometry, which exhibited a robust increase in the population of $CD4^+$ $IL\text{-}17A^+$ T cells (Fig. 6E-G).

Finally, to demonstrate that blocking phenylalanine transport in DCs could reverse this pathogenic axis, LAT1 inhibitor JPH203 was utilized. Notably, T cells cultured in supernatants from DCs co-treated with JPH203 failed to promote a strong Th17 response, as evidenced by the normalized expression of *Rorc*, *Il17a*, *Il17f* and *Il22* (Fig. 6H). In conclusion, these findings demonstrated that phenylalanine acted as a metabolic checkpoint that instructed DCs to create a pro-Th17 microenvironment, thereby sustaining the chronic inflammation characteristic of psoriasis.

Discussion

Within the present study, the results highlighted the key role of phenylalanine in psoriasis, which was associated with amplified inflammatory responses. Elevated phenylalanine was shown to exacerbate skin inflammation through enhanced NF-κB signaling in DCs, ultimately promoting Th17 cell differentiation.

The association between diet and psoriasis has attracted marked attention. However, current dietary guidelines predominantly stem from survey-based studies and lack robust direct evidence (34). To the best of our knowledge, the present study offers the first evidence that phenylalanine, a central dietary component, serves a role in exacerbating psoriasis symptoms. This amino acid is typically present in high levels in red meat and serves as a primary ingredient in aspartame, a commonly utilized artificial sweetener (18). Consequently, a number of patients may unknowingly consume excessive levels of phenylalanine, unaware of its potential hazards. Understanding the effects of phenylalanine on psoriasis is important, especially since individuals with phenylketonuria often experience symptom alleviation through dietary restriction of phenylalanine (35). These findings therefore highlight the importance of dietary considerations in managing psoriasis, potentially empowering patients to make informed dietary choices that could positively affect their condition.

In the present study, a significant increase in phenylalanine concentrations within the skin lesions and peripheral blood of the psoriasis-like mouse model was observed. This finding prompted the hypothesis that inhibition of the transporters responsible for moving phenylalanine into cells may alleviate psoriasis-associated inflammation. JPH203, known as a specific inhibitor of LAT, has been shown in a previous study to ameliorate cutaneous symptoms in a psoriasis-like mouse model when applied topically (36). The present experiments, both *in vivo* and *in vitro*, supported this notion, highlighting the effectiveness of JPH203 in attenuating the psoriasis-associated inflammatory response associated with psoriasis. JPH203 has been studied for its application in inhibiting tumor growth (37) and modulating immune responses by suppressing IL-17-producing T-cell expansion via the PI3K/AKT/mTOR pathway (38), and is currently undergoing clinical trials (39,40). However, the specific molecular mechanisms underlying the anti-inflammatory effects of JPH203 in the context of psoriasis remain to be fully elucidated.

DCs serve a central role in orchestrating immune responses and inflammation in both healthy and diseased states. Studies

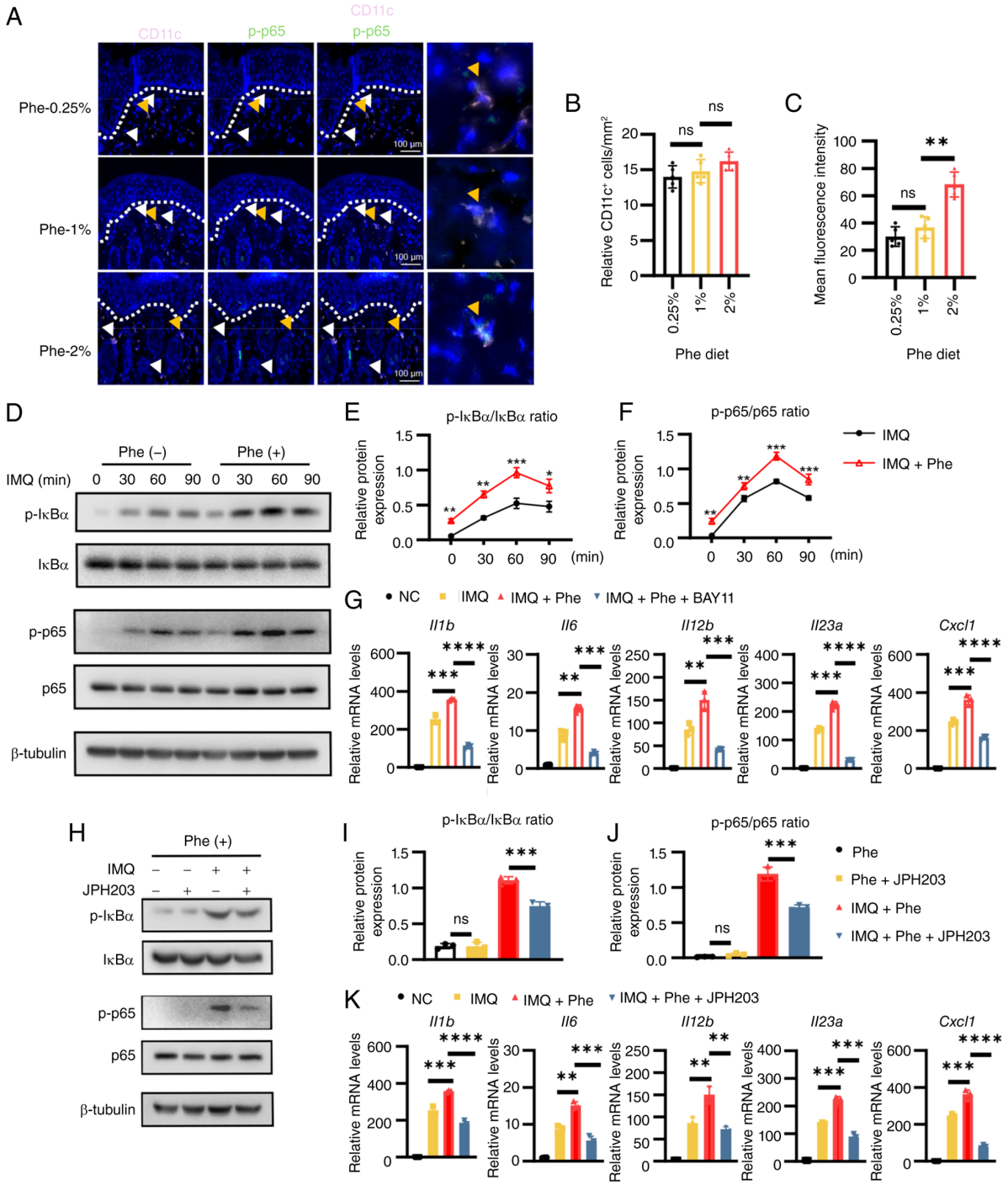

Figure 5. Phe enhances NF-κB signaling activation in dendritic cells to promote pro-inflammatory cytokine production. (A) Representative immunofluorescence images of dorsal skin sections from mice fed different phenylalanine diets (0.25, 1 and 2%). Sections were stained for CD11c (pink), p-p65 (green) and DAPI (blue; scale bars, 100 μm). (B) Quantification of the relative density of CD11c$^+$ cells in the dermis. (C) Quantification of the relative fluorescence intensity of p-p65$^+$cells within the CD11c$^+$ population. (D) Western blotting analysis showing protein expression of the NF-κB pathway in BMDCs. (Expected molecular weights are as follows: p-IκBα, ~39 kDa; IκBα, ~37 kDa, p-p65, ~65 kDa; p65, ~65 kDa; β-tubulin, ~55 kDa). (E,F) Densitometry quantification of (E) p-IκBα/IκBα and (F) p-p65/p65 ratios from the blots in (D). (G) RT-qPCR analysis of pro-inflammatory genes in BMDCs treated with IMQ + Phe, in the presence or absence of the NF-κB inhibitor BAY11-7082. (H) Western blotting analysis of NF-κB activation in BMDCs treated with IMQ + Phe, in the presence or absence of the L-type amino acid transporter 1 inhibitor JPH203. (Densitometry quantification of (I) p-IκBα/IκBα and (J) p-p65/p65 ratios from the blots in (H). (K) RT-qPCR analysis of pro-inflammatory genes in BMDCs treated with IMQ + Phe, with or without JPH203. Data are representative of three independent experiments and presented as the mean ± SEM. Statistical significance was determined by two-way ANOVA (for E and F) and one-way ANOVA (for B, C, G, I, J and K), followed by Tukey's multiple comparisons test. *P<0.05, **P<0.01, ***P<0.001 and ****P<0.0001. Phe, phenylalanine; ns, not significant; BMDCs, bone marrow-derived dendritic cells; p-, phosphorylated; IMQ, imiquimod; RT-qPCR, reverse transcription-quantitative PCR.

have indicated that tryptophan and branched-chain amino acids alter the immunogenicity and tolerance of DCs (41,42). In addition, previous studies have also shown that metal-ion-chelating L-phenylalanine nanostructures activate DCs through the NOD-like receptor family pyrin domain containing 3 inflammasome and the calcium-mediated NF-κB pathway (43). In the

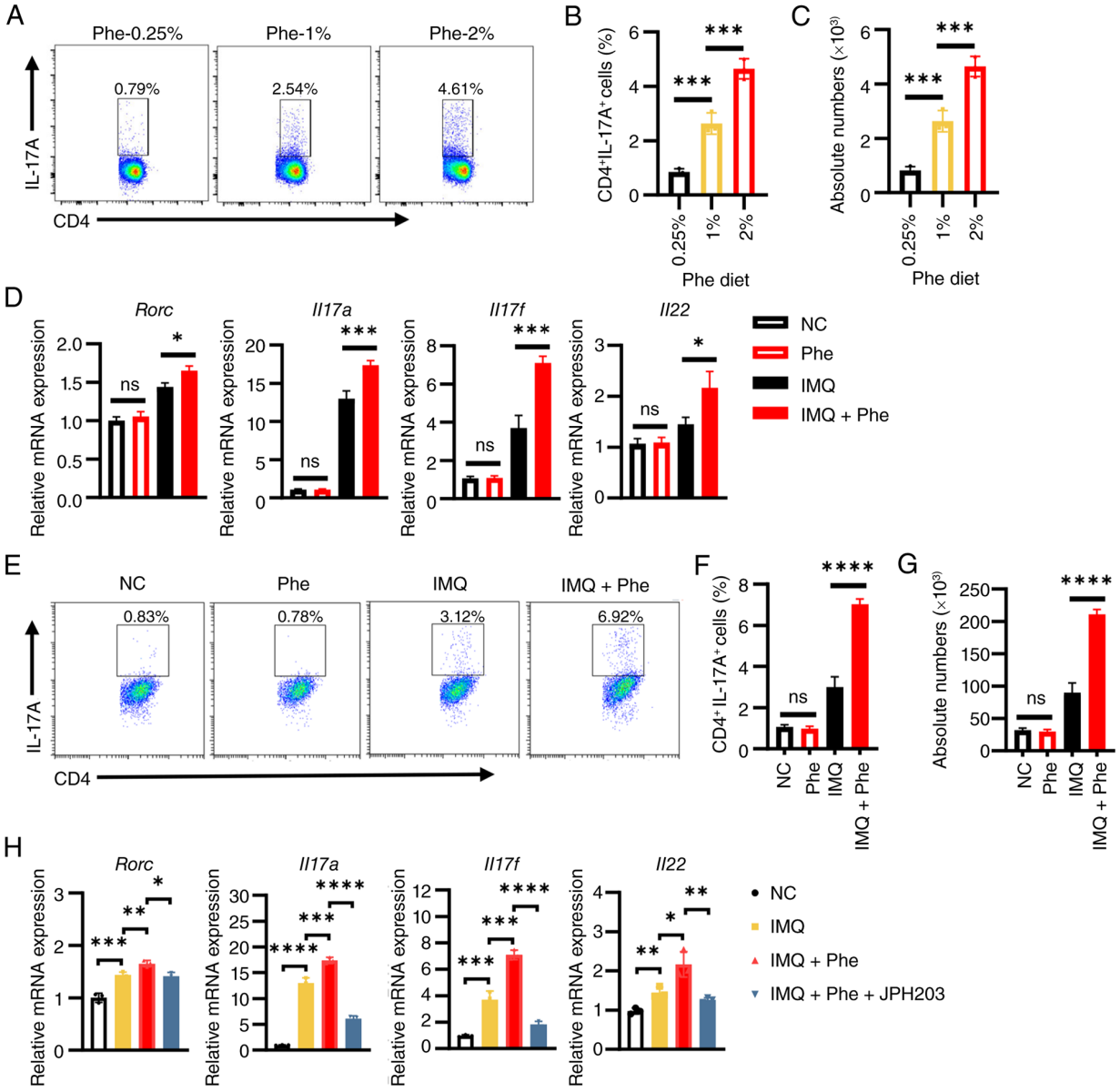

Figure 6. Phe amplifies the Th17 immune response through dendritic cell modulation. (A) Representative flow cytometry plots showing intracellular IL-17A staining in CD4$^+$ T cells isolated from the draining lymph nodes of mice fed diets containing 0.25, 1 or 2% Phe. Quantification of the frequency (B) and absolute number (C) of CD4$^+$ IL-17A$^+$ Th17 cells. (D) RT-qPCR analysis of Th17-associated genes (*Rorc*, *Il17a*, *Il17f* and *Il22*) expression in naïve CD4$^+$ T cells cultured for 3 days in conditioned medium derived from BMDCs treated as indicated. (E) Representative flow cytometry plots of CD4$^+$ IL-17A$^+$ T cells after *in vitro* differentiation in DC-conditioned medium. (F,G) Quantification of the (F) frequency and (G) absolute number of CD4 $^+$IL-17A$^+$ Th17 cells from the *in vitro* assay. (H) RT-qPCR analysis of Th17 markers in T cells cultured in conditioned medium from BMDCs treated with IMQ + Phe, in the presence or absence of the L-type amino acid transporter 1 inhibitor JPH203. Data are representative of three independent experiments and presented as the mean ± SEM. Statistical significance was determined by one-way ANOVA followed by Tukey's multiple comparisons test. *P<0.05, **P<0.01, ***P<0.001 and ****P<0.0001. Phe, Phenylalanine; Th17, T helper cell 17; ns, not significant; RT-qPCR, reverse transcription-quantitative PCR; DC, dendritic cell; BMDCs, bone marrow-derived DCs; NC, normal control; RORC, RAR-related orphan receptor C.

present study, the levels of p-p65 were found to be significantly elevated in a phenylalanine dose-dependent manner. Through transcriptomics and subsequent validation, it was determined that the presence of phenylalanine amplified the inflammatory responses associated with psoriasis in DCs. Furthermore, the inhibition of phenylalanine transport led to suppression of the NF-κB pathway, suggesting that phenylalanine partially exerted its effects by enhancing NF-κB signaling.

Naive T cells can differentiate into Th17 cells when induced by IL-6 and sustain their disease-associated phenotype in the presence of IL-23 (44). Therefore, the present study revealed that exposure to phenylalanine enhanced the production of IL-1β, IL-6, IL-12 and IL-23 in DCs, thus promoting a Th17-polarizing environment (45). Furthermore, it was observed that phenylalanine positively regulated the gene expression of numerous chemokines, such as CXCL1, CXCL2 and CXCL3, in DCs. These chemokines are likely key in recruiting neutrophils and exacerbating tissue inflammation (31). Notably, this phenomenon can be effectively suppressed by JPH203, reinforcing the notion that phenylalanine serves a key role in Th17 differentiation within the context of psoriasis.

A number of limitations in the present study warrant future exploration. Although the present data and recent metabolomics profiling demonstrated elevated phenylalanine levels in the psoriatic lesional skin, the precise mechanisms driving this local accumulation remain unclear. Recent studies have implicated specific transporters, such as SLC16A10 (46) and the ultraviolet B-responsive SLC6A15 (47) in cutaneous phenylalanine uptake. Whether the dysregulation of these transporters contributes to psoriasis lesions requires further investigation. Consequently, while the present study observed marked immune activation, the direct impact of accumulated phenylalanine on keratinocyte dynamics remains to be fully characterized. Given that phenylalanine hydroxylase is transcriptionally upregulated during terminal differentiation (48), future studies should aim to experimentally validate whether exogenous phenylalanine directly modulates keratinocyte proliferation rates. On a molecular level, the direct intermediary mechanisms associating phenylalanine exposure with NF-κB signaling activation, as well as the comprehensive pharmacological pathways through which JPH203 operates in the psoriatic context, have yet to be fully elucidated. Finally, the translational relevance of the present preclinical findings necessitates future validation in human clinical settings.

In conclusion, the present study demonstrated that phenylalanine accumulation elevated the baseline expression of key pro-inflammatory cytokines through the NF-κB signaling pathway, thereby driving the pathogenic IL-23/IL-17 axis. Consequently, the present study revealed a marked association between diet-derived amino acids and immune regulation, offering a viable adjunctive therapeutic strategy for psoriasis.

Acknowledgements

Not applicable.

Funding

The present study was supported by the National Natural Science Foundation of China (grant no. 82373491) and the Zhejiang Province Traditional Chinese Medicine Science and Technology Project (grant no. 2024ZL587).

Availability of data and materials

The data generated in the present study may be found in the China National Center for Bioinformation of the Genome Sequence Archive under accession number PRJCA055303 or at the following URL: (https://ngdc.cncb.ac.cn/bioproject/browse/PRJCA055303) and in the Open Archive for Miscellaneous Data under accession number OMIX014354 or at the following URL: (https://ngdc.cncb.ac.cn/omix/release/OMIX014354).

Authors' contributions

YX and YS conceived the present study. SV and HC designed the present study. YX, ZM, JC and YZ performed the experiments. SC, YW, JP and KL and MC analyzed the data and curated the figures. YX and TY interpreted the data and wrote the manuscript. HC, SV and MC revised the manuscript content. HC, YS and YX confirm the authenticity of all the raw data. All authors read and approved the final version of the manuscript.

Ethics approval and consent to participate

All experimental procedures involving mice were approved by the Animal Research Ethical Committee of the Sir Run Run Shaw Hospital, Zhejiang University School of Medicine (Hangzhou, China; approval no. SRRSH2025-0047).

Patient consent for publication

Not applicable.

Competing interests

The authors declare that they have no competing interests.

References

1. Griffiths CEM, Armstrong AW, Gudjonsson JE and Barker J: Psoriasis. Lancet 397: 1301-1315, 2021.
2. Armstrong AW and Read C: Pathophysiology, clinical presentation, and treatment of psoriasis: A Review. JAMA 323: 1945-1960, 2020.
3. Ghoreschi K, Balato A, Enerbäck C and Sabat R: Therapeutics targeting the IL-23 and IL-17 pathway in psoriasis. Lancet 397: 754-766, 2021.
4. Masson Regnault M, Shourick J, Jendoubi F, Tauber M and Paul C: Time to relapse after discontinuing systemic treatment for psoriasis: A systematic review. Am J Clin Dermatol 23: 433-447, 2022.
5. Torres T, Chiricozzi A, Puig L, Lé AM, Marzano AV, Dapavo P, Dauden E, Carrascosa JM, Lazaridou E, Duarte G, *et al*: Treatment of psoriasis patients with latent tuberculosis using IL-17 and IL-23 inhibitors: A retrospective, multinational, multicentre study. Am J Clin Dermatol 25: 333-342, 2024.
6. Yan L, Wang W, Dong M, Wang R and Li C: Skin metabolic signatures of psoriasis and psoriasis concurrent with metabolic syndrome. J Inflamm Res 18: 505-517, 2025.
7. Yan L, Wang W, Qiu Y, Yu C, Wang R and Li C: Role of glucose metabolism reprogramming in keratinocytes in the link between psoriasis and metabolic syndrome. Int Immunopharmacol 139: 112704, 2024.
8. Hong D, Xiong H, Lu S, Ma J and Shi Z: Metabolic regulation of the immune cell in psoriasis: Mechanisms and interventions. Curr Opin Immunol 96: 102614, 2025.
9. Wan MT, Shin DB, Hubbard RA, Noe MH, Mehta NN and Gelfand JM: Psoriasis and the risk of diabetes: A prospective population-based cohort study. J Am Acad Dermatol 78: 315-322. e311, 2018.
10. Garshick MS, Ward NL, Krueger JG and Berger JS: Cardiovascular risk in patients with psoriasis: JACC review topic of the week. J Am Coll Cardiol 77: 1670-1680, 2021.
11. Herbert D, Franz S, Popkova Y, Anderegg U, Schiller J, Schwede K, Lorz A, Simon JC and Saalbach A: High-fat diet exacerbates early psoriatic skin inflammation independent of obesity: Saturated fatty acids as key players. J Invest Dermatol 138: 1999-2009, 2018.
12. Cappello A, Mancini M, Madonna S, Rinaldo S, Paone A, Scarponi C, Belardo A, Zolla L, Zuccotti A, Panatta E, *et al*: Extracellular serine empowers epidermal proliferation and psoriasis-like symptoms. Sci Adv 8: eabm7902, 2022.
13. He X, Mo Y, Shi P, Xu Y, Zhou M and Zhang T: Tryptophan metabolism in psoriasis and its complications: Future opportunities. J Adv Res 84: 883-894, 2026.
14. Chen C, Hou G, Zeng C, Ren Y, Chen X and Peng C: Metabolomic profiling reveals amino acid and carnitine alterations as metabolic signatures in psoriasis. Theranostics 11: 754-767, 2021.
15. Pohla L, Ottas A, Kaldvee B, Abram K, Soomets U, Zilmer M, Reemann P, Jaks V and Kingo K: Hyperproliferation is the main driver of metabolomic changes in psoriasis lesional skin. Sci Rep 10: 3081, 2020.

16. Miao H, Bai Y, Shen S, Chu M, Miao C, Yang J, Li X, Li L, Shao S, Wang G and Dang E: Biological agent exerts therapeutic effects by reversing abnormalities in amino acid metabolic pathways in psoriasis. Exp Dermatol 33: e15059, 2024.
17. Kamleh MA, Snowden SG, Grapov D, Blackburn GJ, Watson DG, Xu N, Ståhle M and Wheelock CE: LC-MS metabolomics of psoriasis patients reveals disease severity-dependent increases in circulating amino acids that are ameliorated by anti-TNFα treatment. J Proteome Res 14: 557-566, 2015.
18. Zhou Q, Sun WW, Chen JC, Zhang HL, Liu J, Lin Y, Lin PC, Wu BX, An YP, Huang L, *et al*: Phenylalanine impairs insulin signaling and inhibits glucose uptake through modification of IRβ. Nat Commun 13: 4291, 2022.
19. Czibik G, Mezdari Z, Altintas DM, Bréhat J, Pini M, d'Humières T, Delmont T, Radu C, Breau M, Liang H, *et al*: Dysregulated phenylalanine catabolism plays a key role in the trajectory of cardiac aging. Circulation 144: 559-574, 2021.
20. Puig L, Costanzo A, Muñoz-Elías EJ, Jazra M, Wegner S, Paul CF and Conrad C: The biological basis of disease recurrence in psoriasis: A historical perspective and current models. Br J Dermatol 186: 773-781, 2022.
21. Zhang X, Li X, Wang Y, Chen Y, Hu Y, Guo C, Yu Z, Xu P, Ding Y, Mi QS, *et al*: Abnormal lipid metabolism in epidermal Langerhans cells mediates psoriasis-like dermatitis. JCI Insight 7: e150223, 2022.
22. Jaswal A, Kumar A, Patel P and Kurmi BD: Immunometabolic dysregulation in psoriasis: Mechanisms driving inflammation and emerging therapeutic targets. Immunol Invest 55: 948-974, 2026.
23. Chang J, Voorhees TJ, Liu Y, Zhao Y and Chang CH: Interleukin-23 production in dendritic cells is negatively regulated by protein phosphatase 2A. Proc Natl Acad Sci USA 107: 8340-8345, 2010.
24. Guo Q, Jin Y, Chen X, Ye X, Shen X, Lin M, Zeng C, Zhou T and Zhang J: NF-κB in biology and targeted therapy: New insights and translational implications. Signal Transduct Target Ther 9: 53, 2024.
25. McGeachy MJ, Chen Y, Tato CM, Laurence A, Joyce-Shaikh B, Blumenschein WM, McClanahan TK, O'Shea JJ and Cua DJ: The interleukin 23 receptor is essential for the terminal differentiation of interleukin 17-producing effector T helper cells in vivo. Nat Immunol 10: 314-324, 2009.
26. Langley RG and Ellis CN: Evaluating psoriasis with Psoriasis Area and Severity Index, Psoriasis Global Assessment, and Lattice System Physician's Global Assessment. J Am Acad Dermatol 51: 563-569, 2004.
27. Broggi A, Cigni C, Zanoni I and Granucci F: Preparation of single-cell suspensions for cytofluorimetric analysis from different mouse skin regions. J Vis Exp e52589, 2016.
28. Livak KJ and Schmittgen TD: Analysis of relative gene expression data using real-time quantitative PCR and the 2(-Delta Delta C(T)) method. Methods 25: 402-408, 2001.
29. Love MI, Huber W and Anders S: Moderated estimation of fold change and dispersion for RNA-seq data with DESeq2. Genome Biol 15: 550, 2014.
30. Robinson MD, McCarthy DJ and Smyth GK: edgeR: A Bioconductor package for differential expression analysis of digital gene expression data. Bioinformatics 26: 139-140, 2010.
31. Chiang CC, Cheng WJ, Korinek M, Lin CY and Hwang TL: Neutrophils in psoriasis. Front Immunol 10: 2376, 2019.
32. Wohn C, Ober-Blöbaum JL, Haak S, Pantelyushin S, Cheong C, Zahner SP, Onderwater S, Kant M, Weighardt H, Holzmann B, *et al*: Langerin(neg) conventional dendritic cells produce IL-23 to drive psoriatic plaque formation in mice. Proc Natl Acad Sci USA 110: 10723-10728, 2013.
33. Liu T, Zhang L, Joo D and Sun SC: NF-κB signaling in inflammation. Signal Transduct Target Ther 2: 17023, 2017.
34. Ford AR, Siegel M, Bagel J, Cordoro KM, Garg A, Gottlieb A, Green LJ, Gudjonsson JE, Koo J, Lebwohl M, *et al*: Dietary recommendations for adults with psoriasis or psoriatic arthritis from the medical board of the national psoriasis foundation: A Systematic Review. JAMA Dermatol 154: 934-950, 2018.
35. Deon M, Sitta A, Faverzani JL, Guerreiro GB, Donida B, Marchetti DP, Mescka CP, Ribas GS, Coitinho AS, Wajner M and Vargas CR: Urinary biomarkers of oxidative stress and plasmatic inflammatory profile in phenylketonuric treated patients. Int J Dev Neurosci 47: 259-265, 2015.
36. Jiang X, Jiang Z, Huang S, Mao P, Zhang L, Wang M, Ye J, Sun L, Sun M, Lu R, *et al*: Ultraviolet B radiation-induced JPH203-loaded keratinocyte extracellular vesicles exert etiological interventions for psoriasis therapy. J Control Release 362: 468-478, 2023.
37. Hayashi K and Anzai N: Novel therapeutic approaches targeting L-type amino acid transporters for cancer treatment. World J Gastrointest Oncol 9: 21-29, 2017.
38. Cibrian D, Castillo-González R, Fernández-Gallego N, la Fuente HD, Jorge I, Saiz ML, Punzón C, Ramírez-Huesca M, Vicente-Manzanares M, Fresno M, *et al*: Targeting L-type amino acid transporter 1 in innate and adaptive T cells efficiently controls skin inflammation. J Allergy Clin Immunol 145: 199-214.e111, 2020.
39. Lemberg KM, Gori SS, Tsukamoto T, Rais R and Slusher BS: Clinical development of metabolic inhibitors for oncology. J Clin Invest 132: e148550, 2022.
40. Nishikubo K, Ohgaki R, Okanishi H, Okuda S, Xu M, Endou H and Kanai Y: Pharmacologic inhibition of LAT1 predominantly suppresses transport of large neutral amino acids and downregulates global translation in cancer cells. J Cell Mol Med 26: 5246-5256, 2022.
41. Chen J, Liu J and Cao X: Functional and metabolic heterogeneity of dendritic cells in self-tolerance and autoimmunity. Immunol Rev 336: e70068, 2025.
42. Kakazu E, Ueno Y, Kondo Y, Fukushima K, Shiina M, Inoue J, Tamai K, Ninomiya M and Shimosegawa T: Branched chain amino acids enhance the maturation and function of myeloid dendritic cells ex vivo in patients with advanced cirrhosis. Hepatology 50: 1936-1945, 2009.
43. Tan M, Cao G, Wang R, Cheng L, Huang W, Yin Y, Ma H, Ho SH, Wang Z, Zhu M, *et al*: Metal-ion-chelating phenylalanine nanostructures reverse immune dysfunction and sensitize breast tumour to immune checkpoint blockade. Nat Nanotechnol 19: 1903-1913, 2024.
44. Dong C: TH17 cells in development: An updated view of their molecular identity and genetic programming. Nat Rev Immunol 8: 337-348, 2008.
45. Hawkes JE, Yan BY, Chan TC and Krueger JG: Discovery of the IL-23/IL-17 signaling pathway and the treatment of psoriasis. J Immunol 201: 1605-1613, 2018.
46. Luo L, Zeng H, Hu Y, Jiang L, Fu C, Huang J, Chen J and Zeng Q: The amino acid transporter SLC16A10 promotes melanogenesis by facilitating the transportation of phenylalanine. Exp Dermatol 33: e15165, 2024.
47. Zhou S, Ouyang Y, Hu Y, Dai X, Jiang L, Fu C, Wen Y, Huang J, Zhang K, Chen J and Zeng Q: UVB enhances SLC6A15-mediated phenylalanine transport to promote melanogenesis. J Photochem Photobiol B 274: 113329, 2026.
48. Dörner C, Steinbinder J, Sachslehner AP, Sukseree S and Eckhart L: Amino acid metabolism of the skin: Control by specific enzymes and contribution to protective functions. Metabolites 15: 2025.